Supplementary

S1. Nitrogen content of phytoplankton, viruses and zooplankton

Phytoplankton nitrogen content (Eq. S.1) was calculated using cell volume (μm^3) to C content (pg C) and then converted to N content using equations and C:N ratios in Menden-Deuer and Lessard (2000). Nitrogen content of viruses (Eq. S.2) was estimated utilizing volume to C ratio for viral particles in Jover et al., (2014) and C:N ratio. Nitrogen content of zooplankton (Eq. S.3) was calculated from size using equations from Broglio et al., (2003), which converts volume of zooplankton (mm^3) to milligrams of N. This was then converted to units µmol N.

$$n_P = 0.0435 * {vol_P}^{0.811} \quad \text{(S7.1)}$$

$$n_V = 0.0606 * {vol_V}^{0.9283} \quad \text{(S7.2)}$$

$$n_Z = 0.0546 + 0.0137 * vol_Z \quad \text{(S7.3)}$$

S2. Temperature forcing

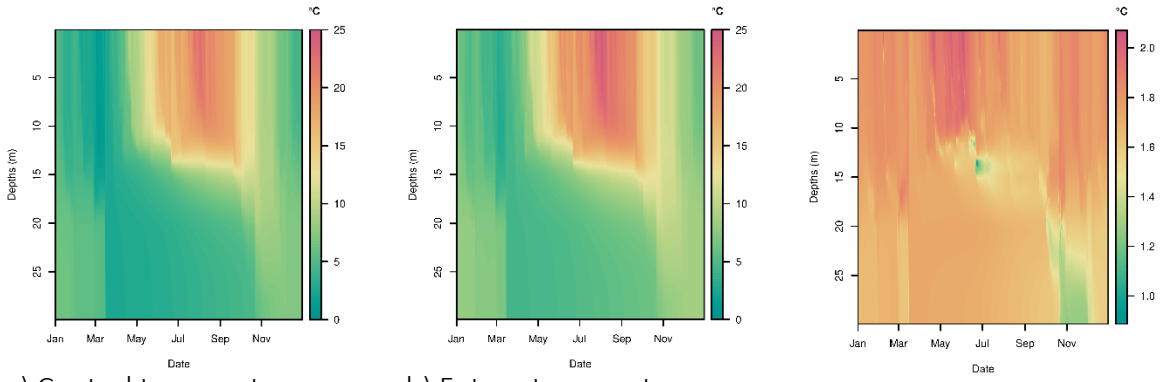

a) Control temperature b) Future temperature c) Change in Temperature

Figure S2: Temperature over depth and the span of a year for a) current conditions and b) future conditions (+2°C), as well as c) the change in temperature over depth and the span of the year between control and future scenario. Red colours indicate a higher, and green values a lower temperature in the future scenario.

S3. Control + Viruses scenario

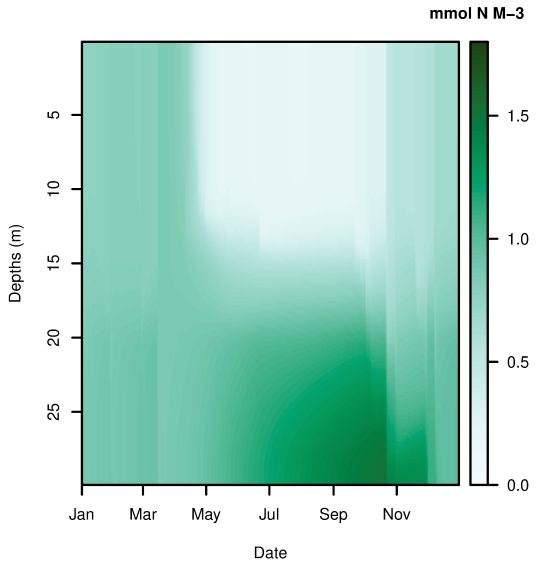

a) Nutrients

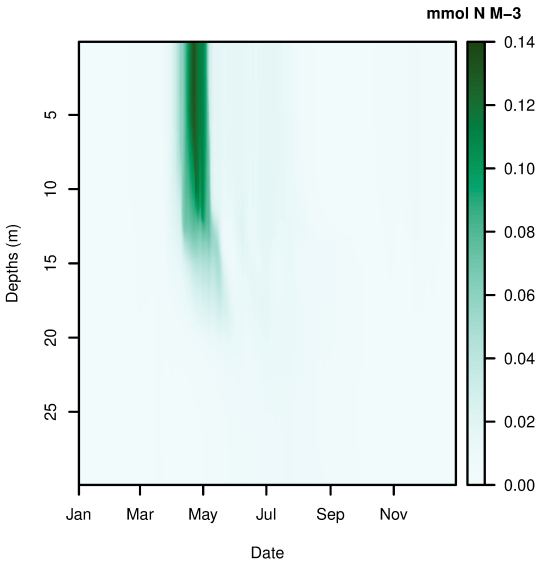

b) Phytoplankton

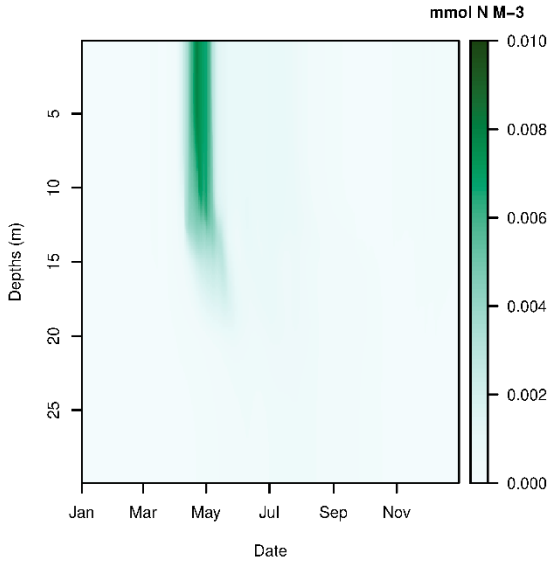

c) Zooplankton

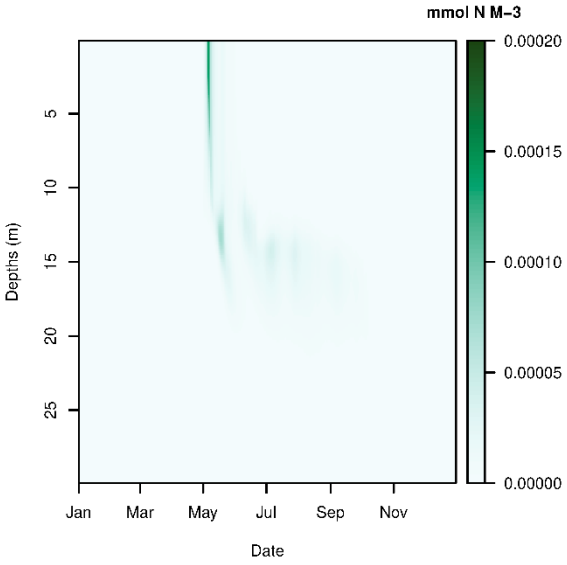

d) Viruses

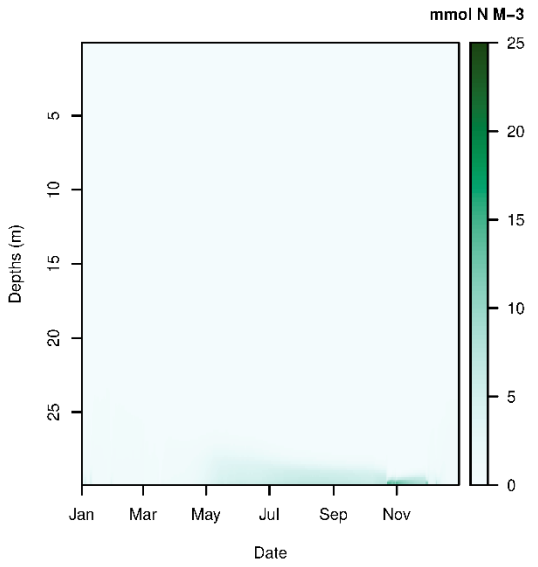

e) Detritus

Figure S3: Seasonal dynamics of a) nutrients, b) phytoplankton, c) zooplankton, d) viruses, and e) detritus for the “Control+Viruses” scenario.

S4. Future scenario without Viruses

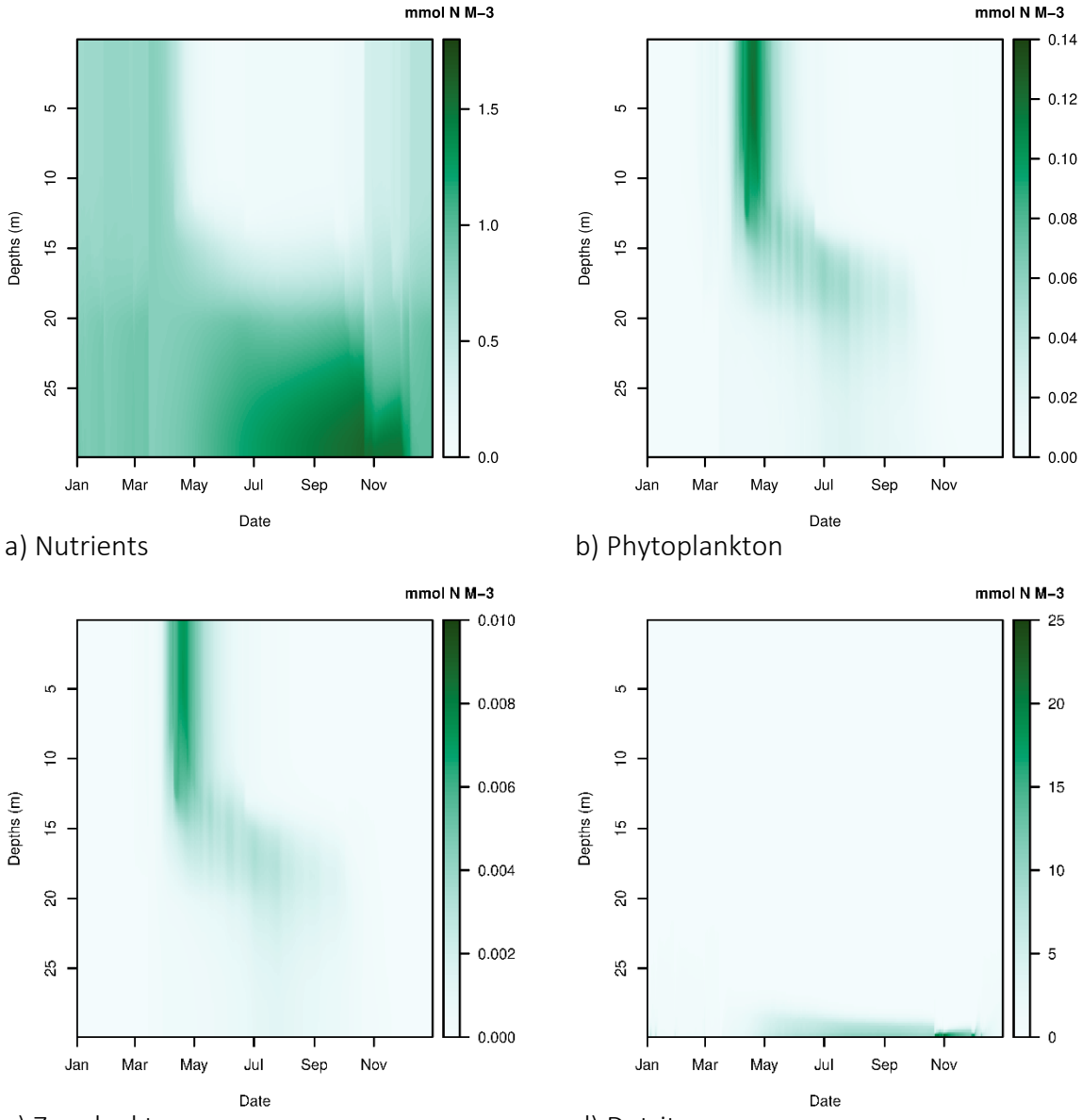

Figure S4: Seasonal dynamics of a) nutrients, b) phytoplankton, c) zooplankton, and d) detritus for the “Future” scenario without viral presence.

S5. Future + Viruses scenario

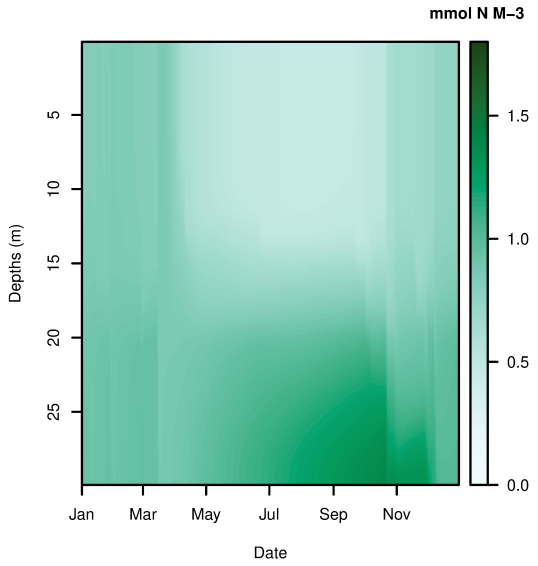

a) Nutrients

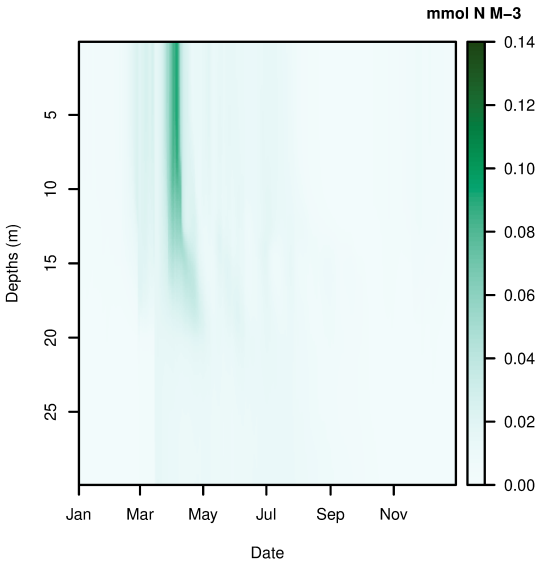

b) Phytoplankton

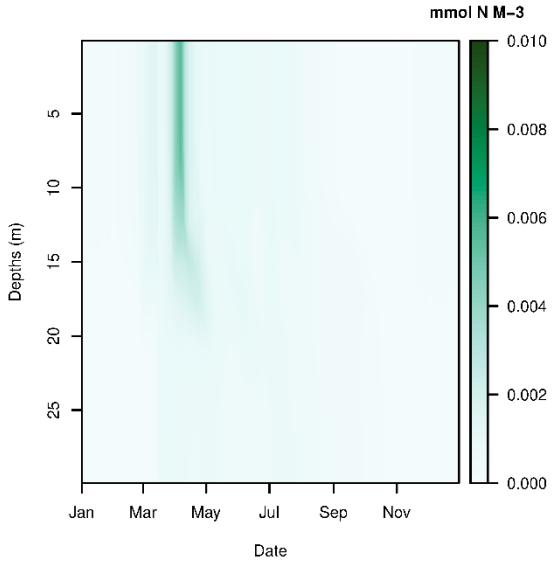

c) Zooplankton

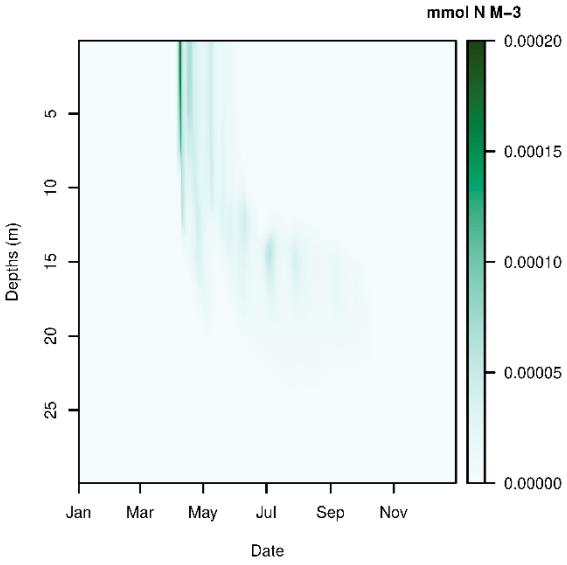

d) Viruses

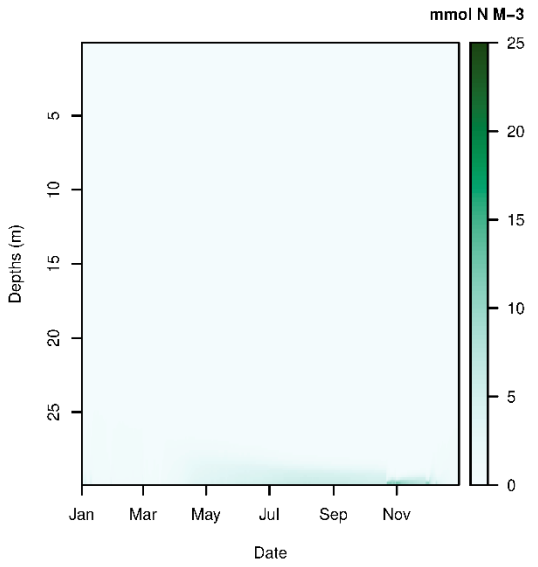

e) Detritus

Figure S5: Seasonal dynamics of a) nutrients, b) phytoplankton, c) zooplankton, and d) detritus for the “Future+Viruses” scenario.

S6. Phytoplankton and zooplankton size data from the Kiel Bight, Baltic Sea, collected from 3-5m depth in 2022.

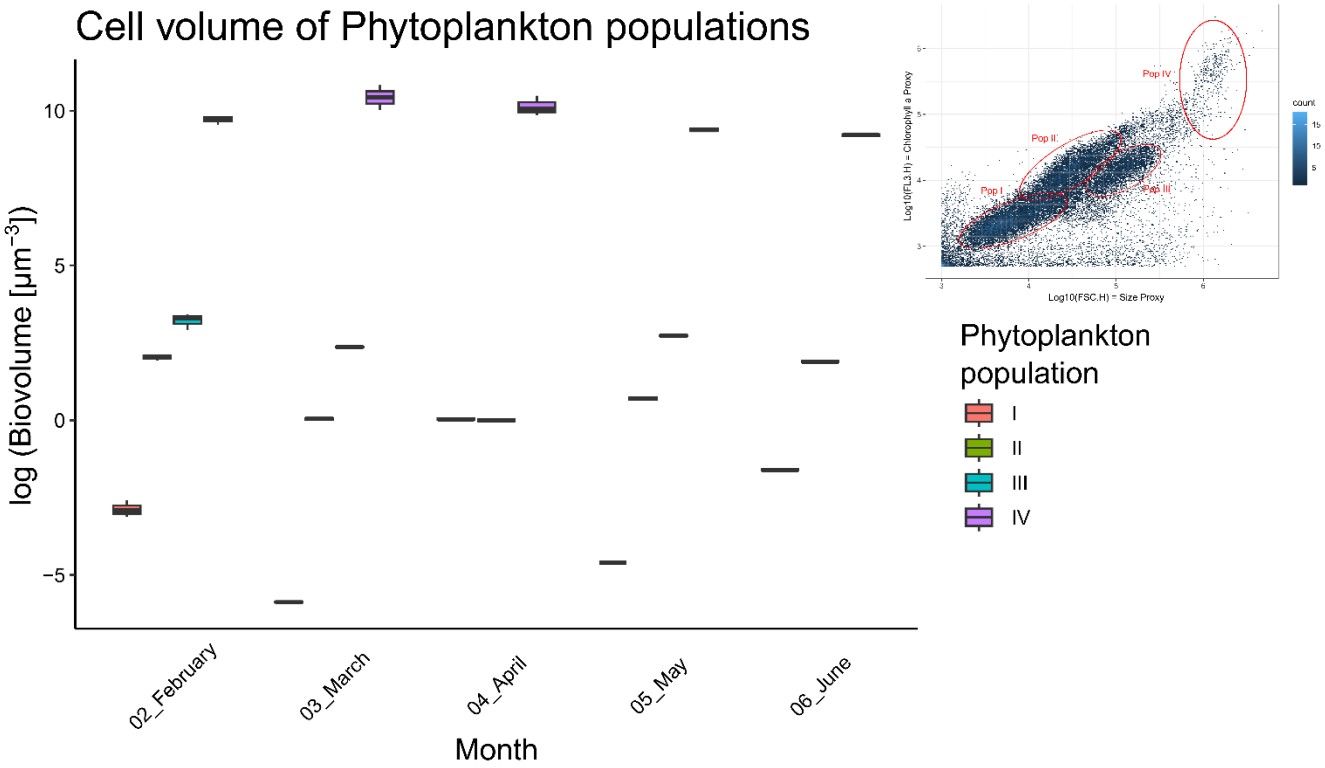

a) Cell volume of phytoplankton populations, populations identified based on flow cytometry (upper right corner). The largest size fraction (diatoms) was used for the phytoplankton compartment in our model.

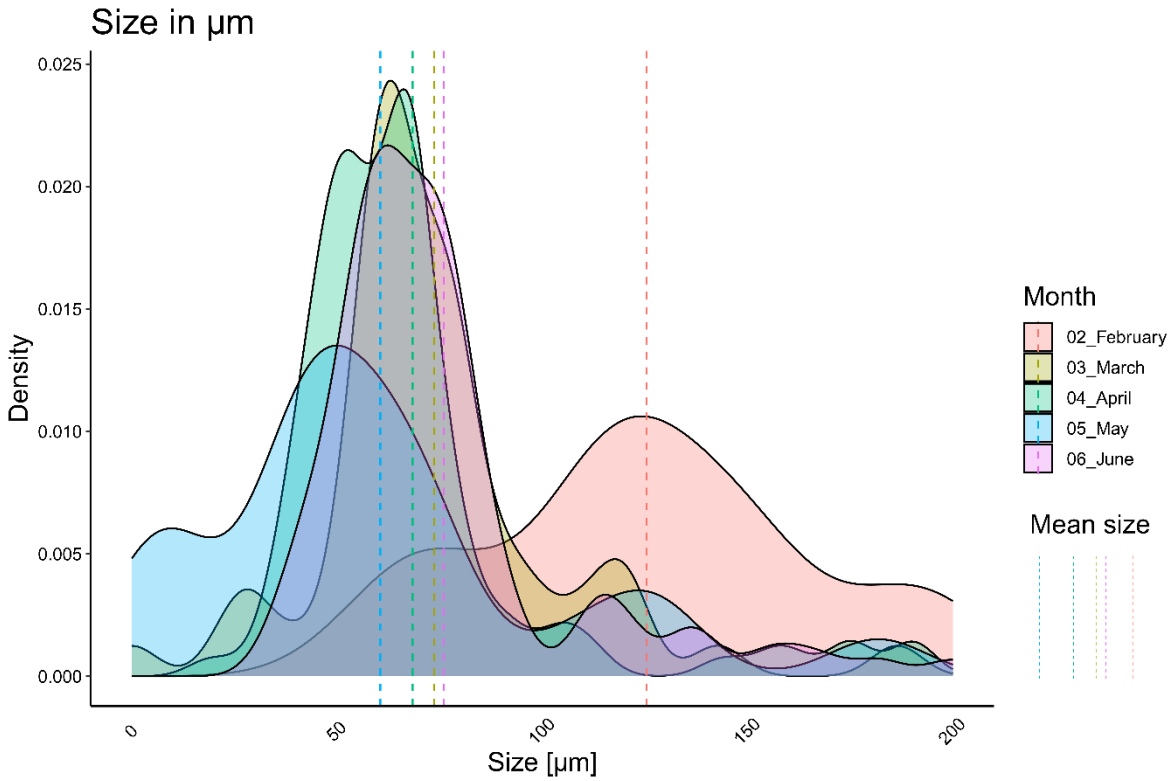

b) Density and size classes of zooplankton across seasons. The zooplankton compartment in our model was described using an intermediate radius of 100 µm.

Figure S6: Cell volume of phytoplankton organisms and radius of zooplankton organisms across seasons.

S7. Phytoplankton mortality due to grazing and viral lysis across seasons, samples from Kiel Bight, Baltic Sea, collected in 3-5 m depth in 2022.

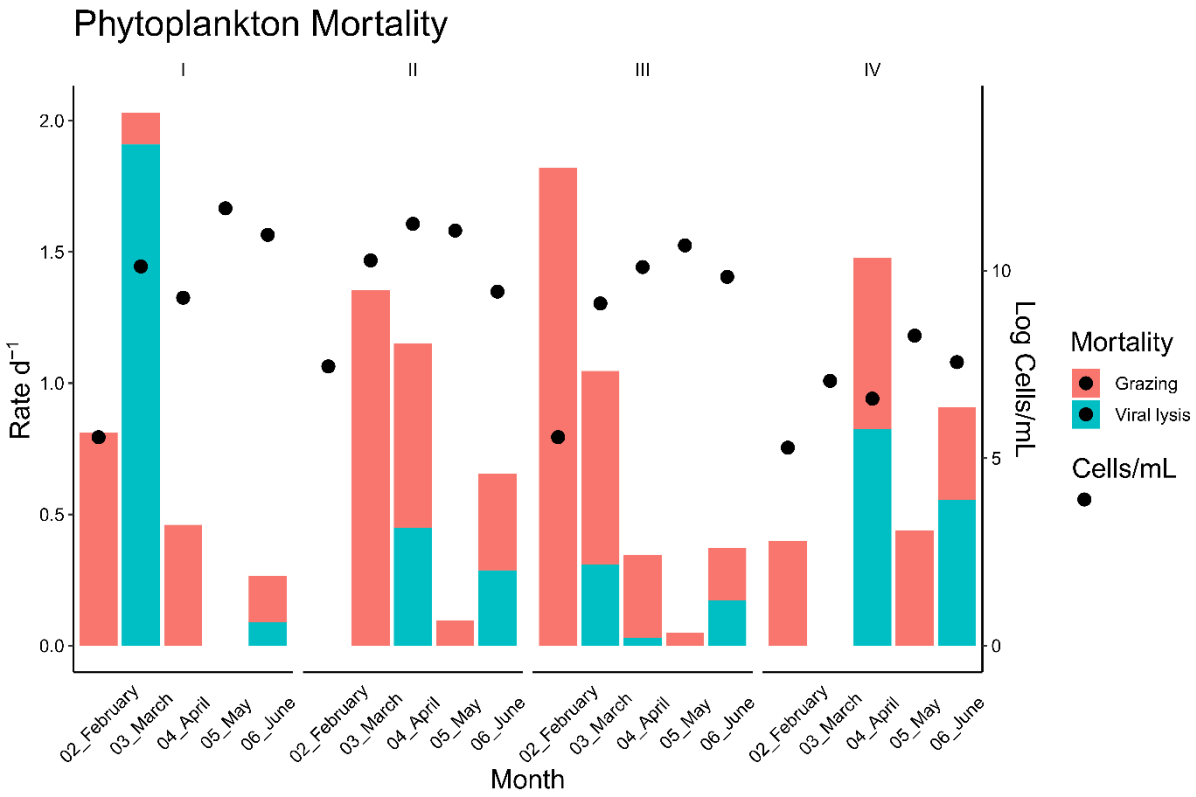

Figure S7: Cell densities (black dots), and mortalities caused by grazing (blue) and viral lysis (red) across seasons. Mortalities were determined following Kimmance (2010). The largest size fraction (diatoms, group IV, see also S6a) shows highest densities in May. Across size fractions, viral lysis dominates as cause for mortality.

S8. Seasonal dynamics of the two-species model including diatoms, picophytoplankton and their respective viruses and zooplankton grazers. Dynamics are shown for the "Future+viruses" scenario

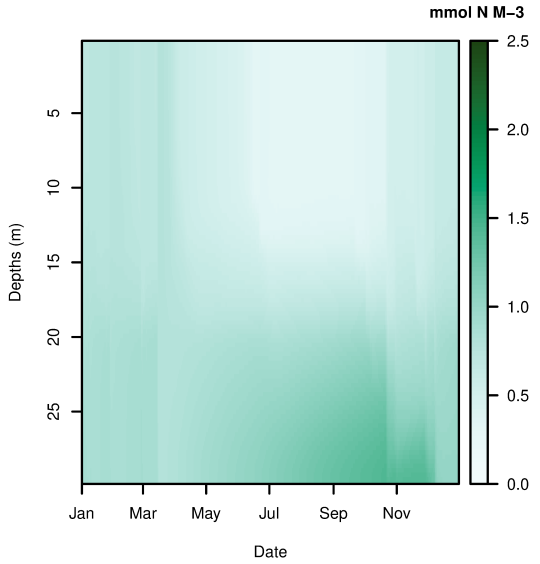

a) Nutrients

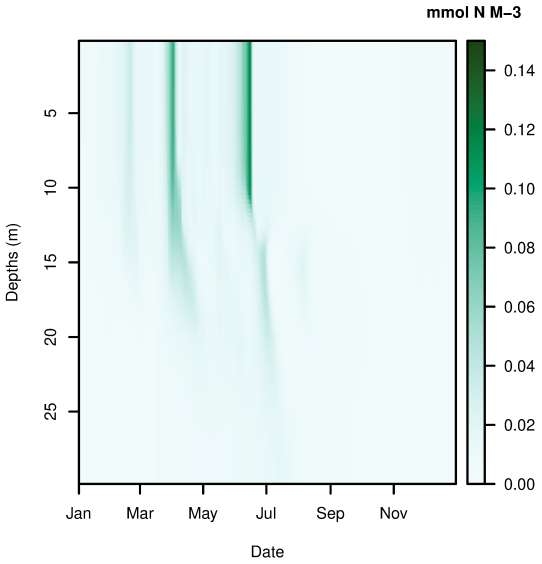

b) Diatom (first) and picophytoplankton (second) bloom

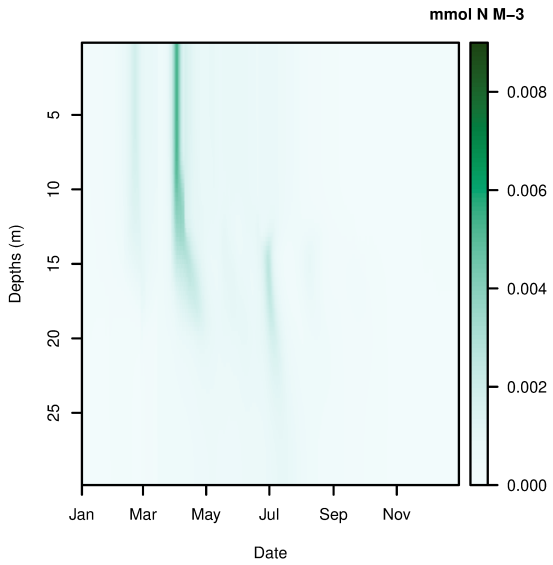

c)Zooplankton

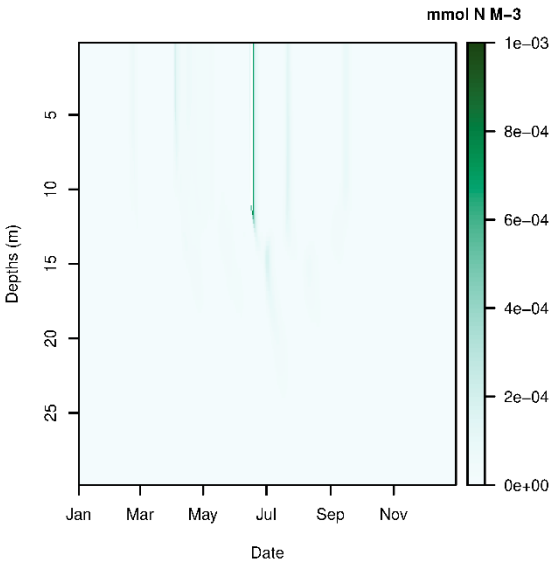

d)Viruses

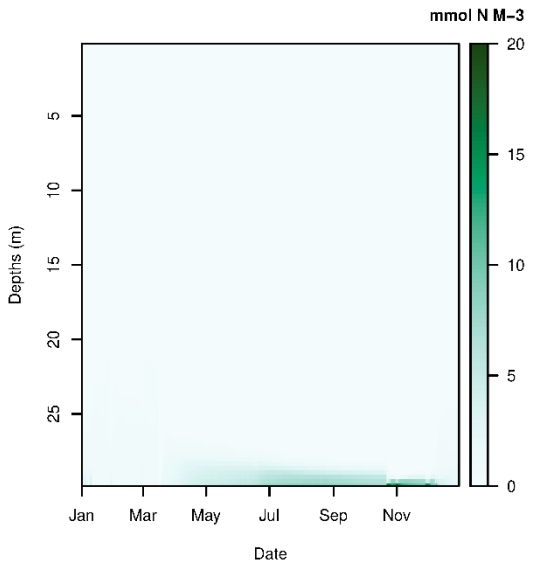

e)Detritus

Figure S8: Seasonal dynamics of a) nutrients, b) phytoplankton, c) zooplankton, and d) detritus for the "Future+Viruses" scenario. The phytoplankton biomass shows the larger diatoms blooming earlier in the year and picophytoplankton with a higher optimum temperature blooming later in the year. While the biomass of viruses targeting diatoms remains limited, the viruses targeting smaller picophytoplankon (second bloom) reach a higher biomass. Zooplankton biomass shows the opposite dynamics, with larger zooplankton preying on diatoms developing a higher biomass than smaller zooplankton.

S9. Annual biomass of all compartments for the two species model

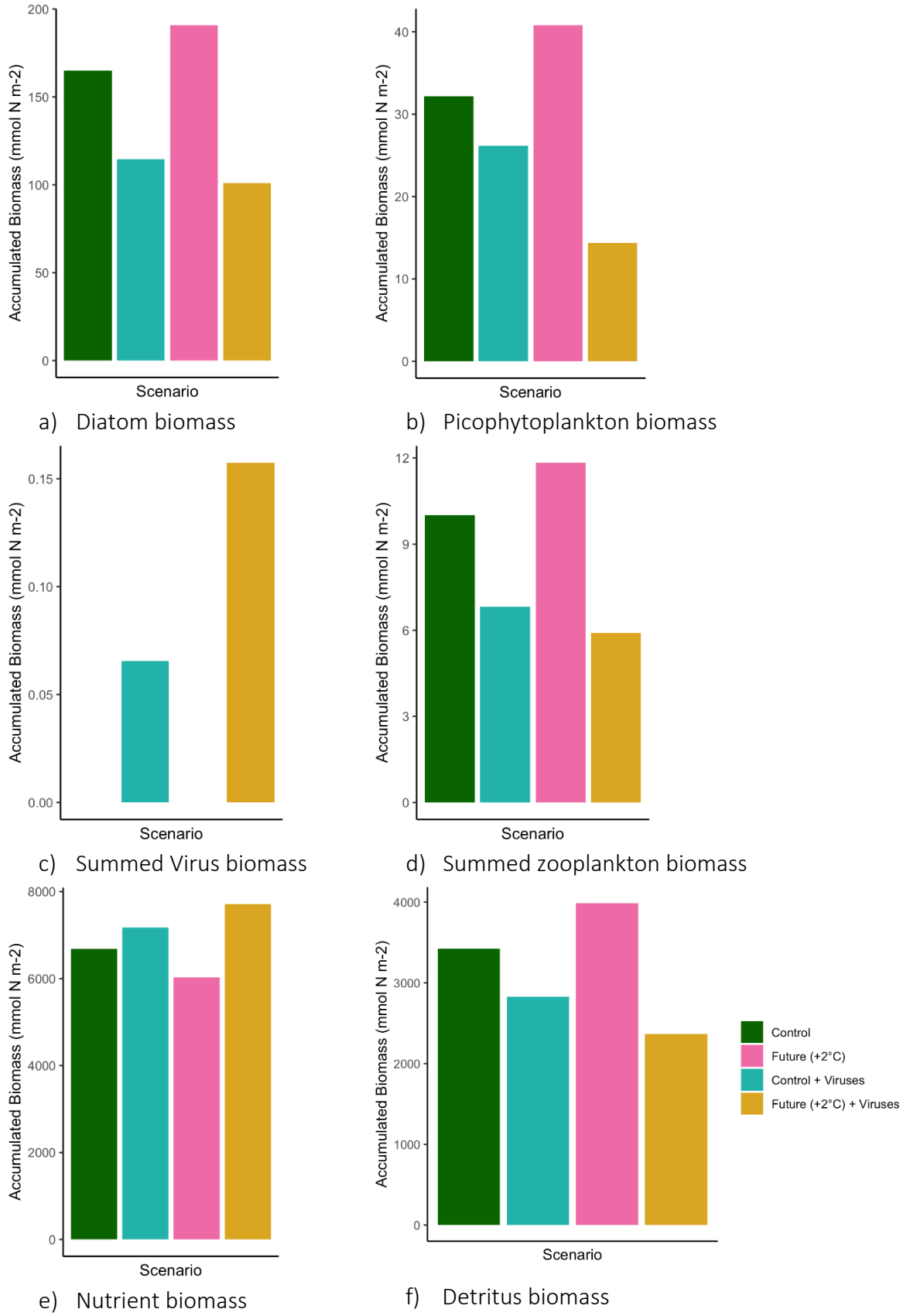

Figure S9: Annual biomass of all compartments integrated over depth and seasons. Scenarios are illustrated using different colours.

References

Broglio, E., Saiz, E., Trepat, I., Alcaraz, M., and Calbet, A.: Estimating zooplankton biomass through image analysis, Mar Biol, 143, 307–315, https://doi.org/10.1007/s00227-003-1094-8, 2003.

Jover, L. F., Effler, T. C., Buchan, A., Wilhelm, S. W., and Weitz, J. S.: The elemental composition of virus particles: implications for marine biogeochemical cycles, Nat Rev Microbiol, 12, 519–528, https://doi.org/10.1038/nrmicro3289, 2014.

Kimmance, S. A. and Brussaard, C. P.: Estimation of viral-induced phytoplankton mortality using the modified dilution method, Limnol. Oceanogr. Methods, 7, 65–73, 2010.

Menden-Deuer, S. and Lessard, E. J.: Carbon to volume relationships for dinoflagellates, diatoms, and other protist plankton, Limnol Ocean., 45, 569–579, https://doi.org/10.4319/lo.2000.45.3.0569, 2000.